The Cryosphere Discuss., https://doi.org/10.5194/tc-2018-101
Manuscript under review for journal The Cryosphere
Discussion started: 20 June 2018

Impact of assimilating a merged sea ice thickness from CryoSat-2 and SMOS in the Arctic reanalysis

Jiping Xie[1], François Counillon[1, 2], and Laurent Bertino[1, 2]

1. Nansen Environmental and Remote Sensing Center, Bergen N5006, Norway
2. Bjerknes Center for Climate Research, Bergen, Norway

*Corrsponding author: Jiping Xie, E-mail: jiping.xie@nersc.no

The Cryosphere Discuss., https://doi.org/10.5194/tc-2018-101
Manuscript under review for journal The Cryosphere
Discussion started: 20 June 2018

Abstract

Accurate forecast of Sea Ice Thickness (SIT) represents a major challenge for Arctic forecasting systems. The new CS2SMOS SIT product merges measurements from the CryoSat-2 and SMOS satellites and is available weekly during the winter months since October 2010. The impact of assimilating CS2SMOS is tested for the TOPAZ4 system - the Arctic component of the Copernicus Marine Environment Monitoring Service (CMEMS). TOPAZ4 currently assimilates a large set of ocean and sea ice observations with the Deterministic Ensemble Kalman Filter (DEnKF).

Two parallel reanalyses are conducted with and without assimilation of the previously weekly CS2SMOS for the period from 19th March 2014 to 31st March 2015. The SIT bias (too thin) is reduced from 16 cm to 5 cm and the RMSD decreases from 53 cm to 38 cm (reduction by 28%) when compared to the simultaneous SIT from CS2SMOS. Furthermore, compared to independent SIT observations, the errors are reduced by 24% against the Ice Mass Balance (IMB) buoy 2013F and by 11% against SIT data from the IceBridge campaigns. When compared to sea ice drift derived from International Arctic Buoy Program (IABP) drifting buoys, we find that the assimilation of C2SMOS is beneficial in the sea ice pack areas, where the influence of SIT on the sea ice drift is strongest, with an error reduction of 0.2-0.3 km/day. Finally, we quantify the influence of C2SMOS compared to the other assimilated data by the number of Degrees of Freedom for Signal (DFS) and find that CS2SMOS is the main source of observations in the central Arctic and in the Kara Sea. These results suggest that C2SMOS observations should be included in Arctic reanalyses in order to improve the ice thickness and the ice drift, although some inconsistencies were found in the version of the data used.

Keywords: Sea ice thickness; Arctic reanalysis; CS2SMOS; EnKF; Innovation; Impact evaluation;

The Cryosphere Discuss., https://doi.org/10.5194/tc-2018-101
Manuscript under review for journal The Cryosphere
Discussion started: 20 June 2018

The Cryosphere Discussions

1. Introduction

Sea ice plays an important role in the Arctic climate system because it prevents the rapid exchange of heat flux between ocean and atmosphere. A decline and a thinning of the sea ice cover has occurred in the past decades (e.g. Johannessen et al., 1999; Comiso et al., 2008; Stroeve et al., 2012). It is expected that this change will have significant impacts on the Arctic Ocean Circulation (e.g. Levermann et al., 2007; Budikova, 2009; Kinnard et al., 2011) and on the future human living environment (Overland et al., 2011; Schofield et al., 2011; Bathiany et al., 2016). The interpretation of such changes is severely hampered by the sparseness of the observations and use of reanalyses that can provide continuous spatio-temporal reconstruction by assimilating existing observations into dynamical models has become increasingly popular tools.

Satellite observation for sea ice concentration (SIC) is available since the 1980s, and has allowed an accurate monitoring of sea ice extent (SIE) in a relative long term. Data assimilation of SIC has been used to improve the evolutions about the sea ice edge (Lisæter et al., 2003; Stark et al., 2008; Posey et al., 2015), but large uncertainty remains in the estimation of sea ice volume as observations of sea ice thickness (SIT) are very sparse. In addition, recent studies (Day et al. 2014; Guemas et al., 2014; Melia et al. 2015) have shown that SIT anomalies take an important role for the Arctic predictability up to seasonal time scale.

Up to the 1990s, the availability of SIT measurement was limited to sparse in situ measurements and submarines data. With the emergence of satellite, continuous estimates of SIT on basin scale have been achieved using radar and laser altimeters from the satellites: European Remote Sensing (ERS), Envisat and the NASA Ice, Cloud and land Elevation Satellite (ICESat). These were used to document the rapid thinning of sea ice in Arctic (Giles et al., 2008; Kwok and Rothrock, 2009; Laxon et al., 2003;).

CryoSat-2 launched in April 2010 has been the first satellite dedicated to measure with high accuracy of the sea ice freeboard, from which the sea-ice thickness can be derived (Ricker et al., 2014; Tilling et al., 2016). The retrieved SIT still contains considerable uncertainty because some approximations are needed as for example in the estimations of the snow depth (using climatology), snow penetration and sea ice density (Kwok, 2014; Kern et al, 2015;

The Cryosphere Discuss., https://doi.org/10.5194/tc-2018-101
Manuscript under review for journal The Cryosphere
Discussion started: 20 June 2018

Khvorostovsky and Rampal, 2016; Ricker et al., 2017). These uncertainties are proportionally large for thin ice (<1 m). Satellite measurements derived from passive microwave radiometer have allowed retrieval of thin sea ice thickness (Martin et al., 2004; Heygster et al., 2009). The Soil Moisture and Ocean Salinity (SMOS) satellite, measures the brightness temperature in a L-Band microwave frequency (1.4 GHz) that can be used for estimating very thin sea ice thickness (Kaleschke et al., 2010; Tian-Kunze et al., 2014), typically bellow 0.5 m. although the overlap between the SMOS and CryoSat-2 estimates is not yet established (Wang et al., 2016), a recent initiative is trying to combine the two complementary data sets (e.g. Kaleschke et al., 2015; Ricker et al., 2017). A merged product of weekly SIT measurements in Arctic from the CryoSat-2 altimeter and SMOS radiometer (referred to as CS2SMOS) is now available online at http://www.meereisportal.de (Ricker et al., 2017). There is a need to test assimilation of this data set and assessment of its potential for reanalysis and operational forecasting.

In this study, the CS2SMOS will be assimilated into the TOPAZ4 forecast system, which is a coupled ocean-sea ice data assimilation system using the Deterministic Ensemble Kalman Filter (DEnKF; Sakov and Oke, 2008). The Ensemble Kalman Filter has previously been demonstrated for assimilation of SIT data (Lisæter et al., 2007) or freeboard data (Mathiot et al., 2012). TOPAZ4 is the main Arctic Marine Forecasting system in the Copernicus Marine Environment Monitoring Services (CMEMS, http://marine.copernicus.eu). Every day, it provides a 10-day forecast of the ocean and biogeochemistry in the Arctic region through the CMEMS portal for the public. It also provides a long reanalysis from 1990 to present – currently 2016 - that is extended every year. By default, SIT products are not assimilated into the reanalysis from TOPAZ4. This reanalysis has been widely used and validated (Ferreira et al., 2015; Johannessen et al., 2014; Xie et al., 2017). Although the Arctic SIT in TOPAZ4 shows spatial coherency with that of ICESat in spring and autumn of 2003-2008, it underestimates SIT (up to 1 m) north of Canadian Arctic Archipelago and Greenland and overestimates it by approximately 0.2 m in the Beaufort Sea (Xie et al., 2017). Even though the SIT from ICESat has been reported too tick by about 0.5 m (Lindsay and Schweiger, 2015), it is undoubted that the SIT from TOPAZ4 has spatial biases. Similar biases for SIT have been reported for other Arctic coupled ocean-ice models (Stark et al., 2008; Johnson et al., 2012; Schweiger et al., 2012; Smith et al., 2015). Xie et al. (2016) have tested assimilation of thin SIT (<0.4 m) from SMOS, and show that assimilation slightly reduced SIT overestimation near the sea ice edge. The recent availability of the weekly SIT from CS2SMOS provides an opportunity for the TOPAZ4 to constrain the SIT error in the Arctic. This study aims at identifying a suitable practical implementation for assimilating C2SMOS data set and assess its usefulness for the Arctic reanalysis. Although it is expected that a better initialisation of SIT anomalies will enhance the predictability of the system, this is beyond the scope of this paper. A similar assessment over the same time frame has been carried out in the Arctic Cap Nowcast/Forecast System (ACNFS) by Allard et al. (2018) revealing significant improvements of bias and RMSE but little changes in ice velocity except in marginal seas. The proposed study in somewhat complementary to Allard et al. (2018) because TOPAZ4 prediction system uses comparatively a more rudimentary sea ice thermodynamics (no explicit ice thickness distribution) but a more advanced ensemble-based data assimilation method – TOPAZ4 uses strongly coupled data assimilation of ocean and sea ice with a flow dependent assimilation method.

Section 2 describes the TOPAZ4 system: namely the coupled ocean and sea ice model, the implementation of EnKF and the observations used for data assimilation and validation. In section 3, we carry an Observing System Experiment (OSE) comparing the two reanalyses: one using the standard observation types used in operational setting and another assimilating the CS2SMOS in addition. Then the performance of the two runs against assimilated and no-assimilated measurements are presented. Section 4 presents the impacts of assimilating the CS2SMOS on sea ice drift and the integrated quantities for sea ice, and quantifies its relative impacts compared to the other observation variables. A summary and discussion are provided in the last Section.

2. TOPAZ system descriptions and observations

2.1 The coupled ocean and sea-ice model

TOPAZ is a forecasting ocean and sea-ice system developed for the Arctic, having been operational since early of the 2000s (Bertino and Lisæter, 2008). It uses the Hybrid Coordinate Ocean Model (HYCOM: version 2.2) developed initially at University of Miami, which has been successfully applied in global and regional oceans (Chassigent et al., 2003; Counillon and Bertino, 2009; Xie et al., 2015). The model grids are constructed using conformal mapping (Bentsen et al., 1999; Bertino and Lisæter, 2008) with a 12-16 km resolution shown in the left panel of Fig. 1. The temperature and salinity along the lateral boundaries are relaxed with a time scale of 20 days to a combined climatology of the Polar Science Center Hydrographic Climatology (PHC: version 3.0, see Steele et al., 2001) and the World Atlas of 2005 (WOA05, ref. Locarnini et al., 2006). A barotropic inflow of Pacific Water is imposed through the Bering Strait, which is balanced by outflowing through the southern model boundary. It has an averaged transport of 0.8 Sv, and varies seasonally with a minimum (0.4 Sv) in January and a maximum (1.3 Sv) in June consistent with the observations proposed in Woodgate et al. (2005).

The model has been coupled at NERSC to a simple sea ice model using one-thickness category. The sea ice thermodynamics is described in Drange and Simonsen (1996), and the ice dynamics uses the elastic-viscous-plastic rheology (Hunke and Dukowicz, 1997) which has a modification (Bouillon et al., 2013)., There is a 0.1 m limit in the model for the minimum thickness of both new ice and melting ice.

2.2 Implementation of the EnKF in the TOPAZ system

The TOPAZ system uses a deterministic Ensemble Kalman Filter (DEnKF, Sakov and Oke, 2008), which solves the analysis without the need to perturb the observations and is regarded as a square-root filter implementation of EnKF. In the DEnKF, if the model state is represented by **x**, the ensemble mean is updated by equation:

$$\bar{\mathbf{x}}^{\mathrm{a}} = \bar{\mathbf{x}}^{\mathrm{f}} + \mathbf{K}(\mathbf{y} - \mathbf{H}\bar{\mathbf{x}}^{\mathrm{f}}), \quad (1)$$

where the superscripts “f” and “a” respectively refer to the forecast and the analysis. Following Xie et al. (2017), the model state vector **x** contains 3-dimensional ocean variables in the native hybrid coordinates (u- and v-

The Cryosphere Discuss., https://doi.org/10.5194/tc-2018-101
Manuscript under review for journal The Cryosphere
Discussion started: 20 June 2018

components of the current velocities, temperature, salinity and model layer thickness), the 2-dimentional ocean variables (u- and v-components of the barotropic velocities, barotropic pressure, and mixed layer depth) and two sea ice tracers (ice area concentration, ice thickness). The assimilated observations are represented by the vector of **y** without perturbation, and the observation operator **H** projects the model variables on the observation space. The misfit between the model and the observation - the bracket term in Eq. 1, is named as innovation. The Kalman gain **K** is calculated by:

$$\mathbf{K} = \mathbf{P^f H^T [H P^f H^T + R]^{-1}} \quad (2).$$

Where $\mathbf{P^f}$ is the matrix of background error covariance, **R** is the matrix of observation error covariance, and the superscript "**T**" denotes a matrix transpose. The background error covariance is approximated from the ensemble anomalies **A** (where $\mathbf{A} = \mathbf{X} - \bar{\mathbf{x}}\mathrm{I}_N$, $\mathrm{I}_N = [1, \ldots, 1]$, N being the ensemble size) as follows $\mathbf{P} = \frac{\mathbf{AA^T}}{N-1}$. Here, $\mathbf{X}$ denotes the ensemble of model states, the observation errors are assumed being uncorrelated (i.e. the matrix **R** is diagonal). While this assumption is not always corrected for some types of observations, it requires the sufficient knowledge about the covariance structure for the observation errors if considering the correlations in **R**. Otherwise, an approximation of the correlated observation error can yield a poor analysis and a diagonal approximation combined with an inflation of the observation error is a reasonable approximation (Stonebridge 2018).

The analyzed ensemble anomaly is calculated as follows (Sakov and Oke, 2008):

$$\mathbf{A^a} = \mathbf{A^f} - \frac{1}{2}\mathbf{KHA^f} \quad (3).$$

The analyzed state matrix $\mathbf{X^a}$ is updated by following:

$$\mathbf{X}^{\mathrm{a}} = \mathbf{A}^{\mathrm{a}} + \bar{\mathbf{x}}^{\mathrm{a}}\mathrm{I}_N \quad (4)$$

In the TOPAZ system, we use an ensemble of 100 members (N=100) to ensure that the sampling error remains small. Localization (local framework analysis) with a radius of 300 km and Gaussian tapering are used in this system.

More details about the practical implementation of the model and perturbations can be found in Sakov et al. (2012), the model errors include joint perturbations of winds, heat fluxes as originally recommended by Lisæter et al. (2007). The precipitation perturbation was increased from 30% to 100%, following a lognormal probability distribution of errors.

2.3 Observations for assimilation and validation

Table 1 overviews of the assimilated observations current in the TOPAZ4 system. Through quality control, they are superobed as described in Sakov et al (2012). The following observations are assimilated sequentially every week: along-track Sea Level Anomaly; in situ profiles of temperature and salinity; gridded OSTIA SST, OSI-SAF sea ice concentration and sea ice drift by satellite. All measurements are retrieved from http://marine.copernicus.eu. For SST and ice concentration, we only retain the analysis at the last day of the assimilation cycle. The sea ice drifts within 2 days in the assimilation cycle from OSI-SAF have been assimilated.

The weekly SITs of CS2SMOS were retrieved from http://data.meereisportal.de/maps/cs2smos/version3.0/n for the period from March 2014 to March 2015. This product is gridded with a resolution of approximately 25 km. Optimal interpolation used by the provider is based on the measurements of CryoSat-2 and SMOS and on their uncertainties considering their spatial covariance. An estimate of the observation error is provided with the data set but it only accounts for the errors related to the merging and interpolation (Ricker et al., 2017). As such it is expected that this observation error is on the low side. Within an EnKF assimilation system, an underestimation of the observation error will lead to a spurious reduction of the ensemble spread and will make the system suboptimal. In the worst cases, the ensemble spread will collapse and the system will diverge. A common practice is to inflate the observation error or to add a term called representative error that accounts for correlated observation error and processes that are not resolved by the model (Desroziers et al., 2005; Karspeck, 2016).

In order to estimate the concerned representative error of the observation error for the SIT, we have carried out a sensitivity assimilation experiment for November 2014, which is independent from our study period. We used the method proposed by Desroziers et al. (2005) to evaluate the observation error suitable in the TOPAZ4 system for assimilating CS2SMOS data. In Desroziers et al. (2005) one can approximate the observation error by the following matrix:

$$\tilde{\sigma}^{o}_{SIT} = \sqrt{\frac{1}{\mathbf{p}}\sum_{j=1}^{p}(\mathbf{y}_j - \mathbf{H}\overline{\mathbf{x}}^{a})(\mathbf{y}_j - \mathbf{H}\overline{\mathbf{x}}^{f})} \quad (5)$$

where *p* is number of data assimilation steps in the sensitivity run (here 4), and $\mathbf{y}_j$ represents the observed SIT from CS2SMOS at the *j*th assimilation time. Here the terms of $\bar{\mathbf{x}}^a$ and $\bar{\mathbf{x}}^f$ represent the ensemble mean of analysis and forecast state. In Fig. 2, the diagnosed observation errors from Desroziers et al. (2005) is much larger than the observation error directly from CS2SMOS. There is a large discrepancy for sea ice from 0.1 to 0.5 m that relates to the underestimated error for the SMOS SIT. It is also noticeable that the discrepancy increases with the ice thickness. In order to palliate for that, we have added a term to the C2SMOS raw error estimate which increases with the amplitude of SIT.

$$\boldsymbol{\varepsilon}_{\mathbf{Offset}} = \min(0.5, 0.1 + 0.15 * \mathbf{d}_{\mathbf{SIT}}) \quad (6),$$

where the $\mathbf{d}_{SIT}$ means the observed sea ice thickness in a grid cell. With the added term, the used observation errors for SIT in the sensitive run are shown by the blue-squared line in Fig. 2. The error is now larger than the Desroziers estimated value. In the work of Oke and Sakov (2008), it was reported that performance does not degrade much when observation error is overestimated while underestimation of the observation error can have disastrous consequence. In the following, we will use the estimated observation error for the CS2SMOS SIT.

3. Observing system experiment (OSE) runs and validations

3.1 Experiment and independent observations for validation

A parallel Observing System Experiment (OSE) is conducted from 19th March 2014 until end of March 2015. The two assimilation runs cover two special time periods: at the onset of ice melting in March-April 2014 following by a free data period of CS2MSOS, and a whole cold season from October 2014 to March 2015. Both runs are 6-hourly forced by atmosphere forcing from ERA-Interim (Dee et al., 2011).

Using the standard observational network in the TOPAZ system (Xie et al. 2017), the control run named the **Official Run** assimilates on a weekly cycle the SLA, SST, in situ profiles of temperature and salinity, SIC and sea ice drift

The Cryosphere Discuss., https://doi.org/10.5194/tc-2018-101
Manuscript under review for journal The Cryosphere
Discussion started: 20 June 2018

(SID) data (See Table 1). The CS2SMOS ice thickness data are weekly averages by grid at 25 km resolution. Considering the different coastlines in the model and observations, we remove the SIT closer than 30 km from the coast. For the SIT, the innovation in Eq. 1 is calculated in terms of sea ice volume:

$$\Delta\mathbf{SIT} = \mathbf{d}_{\mathrm{SIT}} - \mathbf{H}(\bar{\mathbf{h}}_{\mathrm{m}} \times \bar{\mathbf{f}}_{\mathrm{m}}), \quad (7)$$

where $\mathbf{d}_{\mathrm{SIT}}$ is the observed SIT from CS2SMOS as in Eq. 6, $\bar{\mathbf{f}}_{\mathrm{m}}$ is the ensemble mean SIC, and $\bar{\mathbf{h}}_{\mathrm{m}}$ is the ensemble mean ice thickness within the grid cell. Without consideration of the spatial correlation of SIT, the observation error variances (diagonal elements of **R** in Eq. 2) are calculated by the sum of the error specified in the product and the offset term from Eq. 6. Although the minimal thickness in the model is set 0.1 m, the ensemble mean from 100 model members can be as thin as 1 mm, so that we reject the observed SIT for CS2SMOS if equal to 0. Every week, neglecting the time delay, the SITs from CS2SMOS are treated as observations at the analysis time. The associated errors due to the sea ice motions or thermodynamic growth/melt of sea ice remain small within one week compared to the large SIT biases targeted in the present exercise.

In the following, we will investigate the misfits of the forecasted model states by evaluating the bias and the root mean square difference (RMSD) in general:

$$\mathrm{Bias} = \frac{1}{\mathbf{L}}\sum_{\mathbf{i=1}}^{\mathbf{L}}(\mathbf{H}_{\mathbf{i}}\bar{\mathbf{x}}_{\mathbf{i}}^{\mathbf{f}} - \mathbf{y}_{\mathbf{i}}) \quad (8)$$

$$\mathrm{RMSD} = \sqrt{\frac{1}{\mathbf{L}}\sum_{\mathbf{i=1}}^{\mathbf{L}}(\mathbf{H}_{\mathbf{i}}\bar{\mathbf{x}}_{\mathbf{i}}^{\mathbf{f}} - \mathbf{y}_{\mathbf{i}})^2} \quad (9).$$

Where L is the total number of times over the study period, $\bar{\mathbf{x}}_i^{\mathbf{f}}$ is the mean of the model state at the *i*th time, which is comparable to the observations $\mathbf{y}_i$.

Two types of independent observations for SIT are involved for validation. First, the NASA IceBridge Sea Ice Thickness Quick Look data[1], collected in aerial campaigns (Kurtz et al., 2013). Over March and April of 2014 and 2015, the locations of QC'ed observations of SIT are shown as the black-yellow squares in Fig. 1 (left panel). Other independent observations of SIT are obtained from the drifting Ice Mass Balance (IMB) buoys[2] (Perovich and Richter-Menge, 2006). Four IMB buoys (2013F, 2014B, 2014C, and 2014F) are available for a duration

[1] Obtained from http://nsidc.org/data/docs/daac/icebridge/idcsi4/index.htmpl,
[2] http://imb-crrel-dartmouth.org/imb.crrel/buoysum.htm

longer than 5 months. Their trajectories with the beginning positions by the blue markers are also shown in Fig.1 (left).

3.2 Validation against CS2SMOS and innovation diagnostics

The first assimilation time is on the 19th March 2014 and the last is on the 25th March 2015. The monthly SITs for the two OSE runs are compared to CS2SMOS in Fig. 3. The SITs in April 2014 are presented for comparison in the upper panels of Fig. 3. In the Official run, the thick sea ice to the north of the CAA is underestimated but thickens slightly in the Test run: the 2.5 m SIT isoline covers a wider area, in better agreement with the observations. The areas of thinner sea ice north of the Barents Sea, west of the Kara Sea, and the coast of the Beaufort Sea, which were too thick in the Official run, have all been improved.

After summer of 2014, measurements of SIT from CS2SMOS restart at the end of October. Results are presented for November 2014 in Fig. 3: the thick sea ice in the central Arctic has been further improved in the Test run. The thickest sea ice (more than 3 m) is located near the northern coast of Canada instead of north of Greenland in the Official run. In the marginal zones of the East Siberian Sea, the Laptev Sea, and the Kara Sea, the SITs in the Official run is too thin, but is thickened in the Test run. Improvements in these regions are due to the contribution of SMOS, while improvements in the ice pack are mainly due to CryoSat-2.

In the last month of the experimental period (March 2015), the thick sea ice pattern in the Test run, shown as the 2.5 m isoline, is more similar to that of CS2SMOS. The maximal SIT denoted by the 4 m isoline is located north of the CAA in the Test run and in CS2SMOS, while the Official run spreads it out from the northern coast of Canada to north of Greenland. In addition, the SIT north of the Fram Strait is thicker than in the Official run. The SIT is similarly improved near the coast of the Beaufort Sea and to the northwest of Svalbard. As expected with data assimilation, the Test run improves clearly the agreement with the assimilated product. Those improvements are largest in the ice pack and in the marginal Seas, where the model has a considerable deviation compared to the CS2SMOS SITs. On the contrary, the thickness near the sea ice edge is not so significant to be impacted by the assimilation.

The continuous agreement is confirmed quantitatively: misfits of weekly SIT from the two runs are compared with the corresponding CS2SMOS observations. Time series of bias and RMSD, calculated weekly by Eq. 8-9, are shown in the top panel of Fig. 4. At the beginning of the period, the SIT RMSD in the Test run decreases quickly from 0.6 m to 0.4 m before the observations are interrupted, the bias has reduced identically in both runs. After the observations resume in the end of October 2014, the SIT misfits do not increase in the absence of observations during the summer and show lower bias in the Test run, although a RMSD identical to the Official run, before a spike of the errors in early November, which will be attributed to bad observations in Section 4.2. The errors then reduce more in the Test run, both for bias and for RMSD. On average, the thin bias of SIT is decreased from 15 cm to 5 cm by the assimilation of CS2SMOS. The RMSD of SIT is 38 cm in the Test run, reduced by 28.3% relative to the error in the Official run.

The innovation statics taken at assimilation time evaluate whether a data assimilation system is well calibrated. Following the reliability budget analysis formulated in Rodwell et al. (2016), the total uncertainty of the ensemble data assimilation system can be diagnosed as

$$\sigma_{diag} = \sqrt{Bias^2 + \sigma_{en}^2 + \sigma_o^2} \quad (10).$$

Where the *Bias* term is calculated as in Eq. 8 at one assimilation time step, which is convert to the innovation mean (shown as blue-circled lines), σ_{en} and σ_o respectively represent the ensemble spread and the standard deviation of the observation error at the same assimilation time step. If the data assimilation system is reliable, the diagnosed total uncertainty should be close to the Root Mean Square Innovation (RMSI), calculated as in Eq. 9, only taking the model and the observations at assimilation time. Then the time series of SIT innovation statistics are presented in the bottom of Fig. 4 for the Test run throughout the whole time period. The SIT RMSI (red-solid line by inverted-triangle) is initially larger than 0.6 m with a significant bias of 0.3 m (blue solid line with squares). Both are rapidly reducing to 0.4 m and 0.1 m respectively before the summer. In early November 2014, the bias gradually decreases after the aforementioned spike and stabilizes close to zero in the end of 2014, which indicate the benefits of the assimilation compared to the beginning of the experiment. The RMSE stabilizes at a value close to 0.4 m. The innovation statistics for SIC are mostly identical in the two runs (not shown), the mean innovations for SIC vary around ±4% and are most of the time lower than 12%, which is consistent with the evaluation of the TOPAZ4 reanalysis in Xie et al. (2017). It is somewhat disappointing that improvements of ice thickness are of no visible benefit to ice concentration, but a degradation could also have been possible if the thermodynamical model had been over-tuned to an incorrect simulated thickness. It should be noted that the innovation statistics of SST and SLA are also indiscernible in the two runs and not shown either.

3.3 Validation against independent SIT observations

3.3.1 Ice Mass Balance Buoys

Four IMB buoys are available as independent validation of the impact of the assimilation of CS2SMOS. The buoys are drifting in the Canada Basin (Fig. 1), and only one buoy (2013F) lasted during the whole experimental time period shown in the upper panel of Fig. 5. This buoy exhibits the seasonal variability of SIT: it reaches 1.5 m in spring 2014, decreases down to 1.0 m in September and rises again to 2 m in March 2015. The seasonal SIT cycle of the Official run shows excessive seasonal variability, with a thin bias in summer 2014 and a thick bias during the winters. In the Test run (shown as the red-dashed line) the seasonal cycle is dampened and better reproduced. The bias is still quite large around March-April even one year after. It should be noted that the impact of CS2SMOS seems largest in summer, when no observations are available. This indicates the persistent effects of winter thickness to improve the predictability of the summer Arctic sea ice (as in Mathiot et al. 2012). When CS2SMOS is assimilated again in the fall 2014, the Test run initially overestimates the SIT measured at the buoy but is rapidly pulled back to the observation, the subsequent data spike unfortunately raises the SIT shortly after. Still, the time-averaged SIT RMSD for 2013F is reduced from 0.33 m in the Official run down to 0.25 m in the Test run, a reduction of 24.2%.

Two other buoys (2014B and 2014C) cover the early months in the experimental period. At the beginning, the two runs are biased too thick by about 0.5 m and 0.2 m, that are partially reduced with assimilation of CS2SMOS, even after only one month of assimilation. The error along 2014B continues to reduce even after the SIT from CS2SMOS is no longer available, as with the 2013F buoy. For 2014C on the contrary, the assimilation seems to have put the reanalysis on a wrong start by reducing the SIT as the observations indicated more ice growth. For these three buoys the assimilation corrects the mean SIT values but have little influence on the phase of their seasonal cycle. This is probably a model bias which is common for all members in the ensemble.

The buoy 2014F covers the last 6 months of the experimental period, and the SIT growth remains suspiciously weak, from 1.5 m to only 1.6 m in the whole winter, a behavior unlikely to be representative of the area, at least very different from the buoy 2013F. However, the Test Run shows a clear decrease at the start of assimilation, and afterward shows a slower growth of the ice thickness compared to the Official Run. It should be noted that the validation against buoys here is not strictly Lagrangian because the model trajectories differ from the buoys.

3.3.2 IceBridge Quick Look

Another independent observation of SIT with better spatial coverage is the SIT Quick Look data from airborne instruments during NASA's Operation IceBridge campaign (Kurtz et al., 2013). They are available via the National Snow and Ice Data Center (NSIDC), however in the months of March and April only. Note that the airborne SITs are slightly low-biased by about 5 cm compared to in situ measurements as reported by King et al. (2015). Figure 6 shows all observed SITs (upper panel) from IceBridge, collected in March and April of 2014 and 2015, confirming in particular the area of relatively lower SIT to the northeast of Greenland (Section 3.2). The SIT differences to the two OSE runs are presented in the bottom panels. All observed SITs are located in the Canadian Basin and north of Greenland and capture most of the sea ice thicker than 3 m. Sea ice with a thickness between 1~3 m is measured in the Beaufort Sea. The sea ice in the Official run is too thin north of the CAA and north of Greenland, missing more than 1.5 m of ice. In the Beaufort Sea on the contrary, the model is too thick by 0.5 to 1 m. This bias is consistent with Xie et al. (2017), where the TOPAZ4 reanalysis (Official run) was compared to ICESat observation for the period of 2003-2008. This suggests the permanence of these biases due to a combination of errors in the dynamical and thermodynamical evolution of the ice. In the Test run, the biases are slightly reduced by SIT assimilation. On average, the SIT RMSE is 1.08 m, which corresponds to a reduction of 11.5% compared to that in the Official run. Furthermore, the regression of the SIT observations from IceBridge to the two OSE runs is shown in Fig. 7. The Test run shows improved linear correlations to the observation, the offset at the origin is reduced (0.57 m instead of 1 m) and the slope is closer to 1 (1.02 instead of 0.88). However, the model still underestimates the thickest ice observed in IceBridge, with a bias as high as 2 m.

4. Impact of CS2SMOS in the data assimilation system

The above results and assimilation diagnostics confirm that the SIT misfits can be controlled to some degree by assimilation of the CS2SMOS data, without visible degradation of other assimilated variables. In order to better understand the advantages and the limits of assimilating the merged SIT product, we further evaluate the impact of CS2SMOS in the assimilation system: first the repercussions on other sea ice variables and integrated quantities, and then through a quantitative impact analysis of CS2SMOS relatively to other assimilated observation types.

4.1. Impact on the sea ice drift

The EnKF as implemented in TOPAZ updates all the variables in the model state vector, using flow-dependent multivariate covariances from the ensemble members (Eqs. 1 and 2). The direct assimilation update of ice drift is however short-lived: the ice drift vectors quickly readjust to wind forcing after assimilation, so the ice drift changes are mostly caused by dynamical readjustments, related to the updated ice thickness and ice concentrations.

The force balance per unit area is formulated by the two-dimensional momentum equation as follows:

$$\mathbf{m}\frac{\partial \mathrm{u_i}}{\partial \mathbf{t}} = -\mathbf{mf}\mathrm{k} \times \mathrm{u_i} - \mathrm{mg}\nabla\boldsymbol{\eta} + \boldsymbol{\tau}_{\mathbf{ai}} + \boldsymbol{\tau}_{\mathbf{wi}} + \nabla\cdot\boldsymbol{\sigma}_{\mathrm{i}} \tag{11}$$

where $\mathbf{u}_i$ is the drift vector. The first term at right-hand side represents the Coriolis force, and *f* is the Coriolis parameter. The tilt effect is represented by the second term where η is the sea surface height and *g* is the gravity acceleration. On the sea ice, the wind and ocean stresses are $\boldsymbol{\tau}_{\mathbf{ai}}$ and $\boldsymbol{\tau}_{\mathbf{wi}}$, respectively. The ice rheology is the last term calculated by the divergence of the internal stress tensor σ_i. The mass $\boldsymbol{m}$ in Eq. 11 is the total mass of ice and snow per grid cell:

$$\mathbf{m} = \rho_i \mathbf{h}_i + \rho_s \mathbf{h}_s \tag{12}$$

where h_i and h_s represent the thicknesses for sea ice and snow respectively. The ice and snow densities of ρ_i and ρ_s are constant here. By the first order approximation, the drift velocity of sea ice is mainly controlled by 1) the interactions of atmosphere-sea ice, 2) the interactions of ocean-sea ice and 3) the internal sea ice forces as the last three terms to the right of Eq. 11 (Hibler 1986; Hunker and Dukowicz, 1997). Olason and Notz (2014, thereafter called ON14) show from observations that ice thickness is the main driver changes of ice drift in winter (December to March), while the concentration is the main driver in summer (June to November) and ice drift may increase independently from concentration of thickness in transition periods due to increasing fracturing. In the TOPAZ model, the sea ice dynamics assume a viscous-plastic material with an adjustment mechanism at short timescales by elastic waves (called EVP, Hunke and Dukowicz, 1997). Following the EVP rheology in Hibler (1979), the stress tensor σ_i as in Eq. 11 is forced by a pressure term which takes a function of the sea ice thickness and concentration only.

$$\mathrm{P} = \mathrm{P}^{*}\mathrm{h}exp(-C(1-A)), \tag{13}$$

Where C and P* are empirical constants, h is SIT, and A is sea ice concentration. ON14 thus show that this type of rheology is able to reproduce the changes of ice drift whenever they are related to changes of concentration and thickness, although not the changes during the transition periods. The sensitivity of ice drift to ice thickness can be directly adjusted by tuning the value of P* in Eq. 13 (see for example Docquier et al., 2017) The ice thickness does as well have an influence on the ice concentrations in the summer due to melting, but this influence is limited in TOPAZ4 by the assimilation of ice concentrations. The winter months in the seasonal cycle (see Figure 6 in ON14)) indicate that a 10% increase of ice thickness can reduce the ice drift by 9%. Areas of thinner ice are much more sensitive (see Figure 5 in ON14) and therefore the above numbers are subject to possible biases of ice thickness. The sensitivity on seasonal time scales may also differ from the sensitivity on a weekly time scale (that of the TOPAZ assimilation cycle).

The evaluation in Xie et al. (2017) shows the model drift of sea ice is overestimated by 2 km d^{-1} on average on the Arctic with an uncertainty of 5 km d^{-1}. The thickness of thick ice is also too thin, consistently with the too fast drift (Figures 14 and 17 in Xie et al., 2017). So the assimilation of ice thickness can improve the ice drift by dynamical model adjustment, as we expected. Figure 8 shows the monthly differences of the 2 days sea ice drift (SID) compared to the OSI-SAF estimates based on passive microwave data in April 2014, December 2014 and January 2015 (see Table 1). The SID in the Official run is too fast in the central Arctic where the SIT was found too thin in Fig. 3. Despite of the relative small assimilation impact of CS2SMOS on the SID, there are improvements are across the Arctic in all winter months. The RMSD of sea ice drift speed is reduced about 0.2-0.3 km d^{-1} in April 2014 and January 2015. On the other hand, we acknowledge that the drag coefficients between sea ice and other medias had been tuned to best match the sea ice drift with the Official run even with a biased SIT. Consequently, further improvements should be achieved if these parameters were “retuned” with the Test run.

To evaluate the potential impact of assimilating the SIT from CS2SMOS on the sea ice motion, we further utilize the data set from the International Arctic Buoy Program (IABP) which began in 1990s to monitor ice motion throughout the Arctic Ocean. The buoy data files are collected from ftp://iabp.apl.washington.edu/pub/IABP. In this study, the 3-hourly data from IABP are used, keeping trajectories longer than 30 days with more than 5 positions per day. Based on these 3-hourly trajectories, the daily drift speed is calculated by the total drift distance divided by time. Moreover, buoys trajectories are filtered by sea ice concentration (>0.9) and the SST (<-1 °C) as simulated by TOPAZ4 at their locations. During the experimental time period, there are 194 buoys giving 27,437 daily drift speeds in the whole Arctic, shown in the right panel of Fig. 1.

To avoid unresolved coastal effects, we restrict the dataset to the area shown by the red line in this panel. The waters nearer than 50 km from the coast are excluded if shallower than 30 m, reducing the dataset to 22,329 observations from 152 buoys. The speed distribution for daily drift of sea ice from IABP is shown by histogram in Fig. 9a. In the central Arctic, the averaged drift speed is about 10.6 km d^{-1} (consistently with Allard et al., 2018) and most speeds (95%) are slower than 24 km d^{-1}. The concerned speed distributions of sea ice drifts in the two runs of Official and Test are very similar with the observed by IABP. Their difference about the drift distributions is not obvious for the two runs in Fig. 9b, both indicating a 2 km d^{-1} too slow drift, although the comparison to the OSI-SAF product showed too fast drift and gave a clear advantage to the Test run. This inconsistency indicates a poor representativity of the IABP buoys in the period of our runs. For our particular purpose, Fig. 1 shows that the IABP buoys do not sample at all the Central Arctic where the SID misfits are largest and the model drift is overestimated significantly. This poor coverage of IABP buoys may as well explain why the SID comparisons in Allard et al. (2018) were inconclusive.

However, Fig. 9c shows that the distributions of SITs at the IABP buoys locations have been significantly adjusted between the two runs: The thick sea ice (>2.2 m) becomes more abundant in the Test run and the relatively thin sea ice (0.5-1.7 m) more abundant in the Official run. The averaged SIT thus increases from 1.48 m to 1.58 m in the Test run.

4.2 Impact on the sea ice extent and volume in the central Arctic

As above shown in Fig. 3, the Arctic SIT has been improved and the drift slightly improved accordingly in the central Arctic when compared to observations. But the observation coverage does necessarily warrant the physical consistency of basin-scale integrated quantities. The impact of CS2SMOS on the Arctic-wide sea ice extent (SIE) and the sea ice volume (SIV) are investigated for the two runs and compared with the estimates from CS2SMOS and OSI-SAF respectively. Due to differences of resolution and land mask (especially important in the Canadian Archipelago), we focus on the central Arctic domain shown as the redline in the right panel of Fig. 1, excluding parts of the marginal seas.

Figure 10 shows the time evolutions of SIE and SIV in the two runs of Official and Test. Both are calculated by daily averages in the two model runs. The SIE is classically calculated in the area where the SIC requires no less than 15% in the Central Arctic. The SIE shows the expected seasonal cycle with the minimum (close to 3x10^{6} km$^{2)}$ in September 2014 and saturates at a maximum value corresponding to the area of the Central Arctic region (around 6x10^6 km^2) from January to March. The timing of the minimum and maximum from the two model runs agree very well with the observed in OSI-SAF and CS2SMOS (using the weekly concentration within the CS2SMOS product). We can also notice the impact of the weekly assimilation cycle that causes some "sawtooth" discontinuity and indicates that the model tends to both melt too fast in August and freeze too fast in September-October. Overall the SIE differences between the two runs (about 8,000 km^2) are indiscernible during the experimental time period.

The time evolutions of the SIV in the two runs show larger differences in the lower panel of Fig. 10. The maximum in the Test run is close to 12x10^3 km^3 in April-May of 2014 and again end of March 2015, and the minimum is close to 5x10^3 km^3 in September 2014. On average, the SIV difference in the two OSE runs is about 1,000 km^3, with lower volume in the Official run. It shows the assimilation of the CS2SMOS results in the SIV increase about 8% relative to that in the Official run over the one year. The signature of the assimilation cycle is generally less pronounced than on SIE, except in August 2014 due to the SIC updates which are positively correlated to SIT in the summer (as noted in Lisæter et al., 2003). Compared with the observed SIV from the weekly CS2SMOS, the underestimation is significant at beginning of the runs (about 3x10^3 km^3), but corrected by one third through the first month of assimilation of CS2SMOS. When the CS2SMOS data are missing, the gap between the two runs remains constant throughout the summer due to the long memory of winter ice, as previously noted with the assimilation work of ICESat SIT data in Mathiot et al. (2012). After the end of the "summer break"，the SIV from the Test run has been in a better agreement with the first observed SIV from CS2SMOS. This indicates that the TOPAZ4 Official run has underestimated SIV due to the history of the reanalysis but not as a systematic tendency of the model system. The SIV estimates from observations occasionally present sudden discontinuities that seem unrealistic for a large integrated quantity such as the SIV of the central Arctic area. These discontinuities are larger than what the data assimilation system would expect based on the assumed observation error statistics given above. But the time series indicate that the EnKF does, as the

The Cryosphere Discuss., https://doi.org/10.5194/tc-2018-101
Manuscript under review for journal The Cryosphere
Discussion started: 20 June 2018

The Cryosphere Discussions
Open Access

name indicates, filter out part of the discontinuities so that only the major spike in early November 2014 causes a discontinuity in the Test run. Fig. 11 shows that the spike corresponds to a large homogeneous increase of SIT in all marginal seas between 26th Oct and 2nd Nov 2014, then a large decrease in the following week.

4.3 Quantitative impact for the observational network

A data assimilation system can only honour a new source of information at the expense of the other data sources. The introduction of SIT here also enters in competition with the observations already assimilated. The value of the Degrees of Freedom for Signal (DFS) is commonly used to monitor the relative impact of different observations in a data assimilation system (ref. Cardinali et al, 2004; Rodgers 2000; Xie et al, 2018), and is calculated as follows:

$$\mathrm{DFS} = tr\left(\frac{\partial \hat{\mathbf{y}}}{\partial \mathbf{y}}\right) = tr\left\{\frac{\partial[\mathbf{H}(\bar{\mathbf{x}}^{\mathrm{a}})]}{\partial \mathbf{y}}\right\} = tr(\mathbf{KH}) \quad (14).$$

Where $\hat{\mathbf{y}}$ is the analyzed observation vector, the observation operator **H** is same in Eq. 1, and the term *tr* is the trace operator (see Sakov et al. (2012) for an application to the TOPAZ4 system with the EnKF). The DFS is easily calculated and stored while performing the analysis with ensemble data assimilation. It measures the reduction of uncertainty caused by a given observation type expressed as a number of equivalent degrees of freedom. A DFS of 0 means the observation without impact at all, and a DFS equals to the total number of degrees of freedom would indicate that the observation has so much impact that it has collapsed the ensemble to a single value. As the analysis is solved either in observational space or in ensemble space (depending on which is computationally cheapest), the DFS cannot exceeds the smaller of the ensemble size (100 in the present application) and the number of observations used for the local assimilation. Eq. 14 reveals that the DFS depend on the observation error statistics but not on the actual observation values. The DFS quantity is linear and can be split by observation types and accumulated in time periods. The averaged DFS for the *k*th type of observation can then be noted by $\overline{DFS_k}$, and thus a corresponding Impact Factor (IF) is defined as:

$$\mathrm{IF_k} = \frac{\overline{DFS_k}}{\sum_{i=1}^{O} \overline{DFS_i}} \times 100\% \quad (15).$$

The Cryosphere Discuss., https://doi.org/10.5194/tc-2018-101
Manuscript under review for journal The Cryosphere
Discussion started: 20 June 2018

Where *o* represents the number of different observation types assimilated in this time period. IF_k represents the relative impact of the *k*th type of observations with respect to the whole observation network.

Figures 12 and 13 show the IF_k for different observations assimilated in the Test run averaged in two typical months: in November 2014 and in March 2015. The SIC impacts are dominant where close to the sea ice edge and in the CAA region in the November, with an average IF of 22.7% in the whole Arctic. The SIT impact from CS2SMOS is largest in the central Arctic in November 2014. A relatively smaller impact (>20%) is also noticeable in north of the Barents Sea and west of the Kara Sea. In the open ocean, the SST and SLA have the largest impact. Temperature and salinity profiles have locally an important effect in the ice-covered Arctic, where a few of ice-tethered profilers (ITP) are available and the uncertainty is large. Xie et al. (2016) applied the same DFS method to evaluate the impact of thin SIT from SMOS only. The present results reveal, as expected, much larger impacts of CS2SMOS SITs in the central Arctic, with only a few isolated dips where the ITP profiles are available. The IF is higher where the ice is thicker, even though the observation error increases as a function of ice thickness. It indicates that the ensemble background errors increase even more than the observation errors in thick ice by temporal accumulation of model errors. For example, errors in precipitation grow as the snow accumulates in the Fall, and the resulting inter-member variability of snow cover causes inter-member variability of SIT due to the thermal isolation effect of snow.

In March 2015, CS2SMOS has again a large impact in the central Arctic relative to other assimilated observations even though previous literature indicates a lower impact in the midst of winter than when the ice is growing (Mathiot et al., 2012). The relative IF of SIT indeed remains high even though the absolute DFS is decreasing, due to the lower impact of other assimilated observations, in particular SIC (Lisæter et al., 2003). On average, the IF value of CS2SMOS is about 40%. The high values (>40%) are clearly separated into two areas: one is to the north of the CAA and Greenland; another following the inner side of the sea-ice edge in marginal ice zones. The former is primarily a CryoSat-2 contribution, while the latter corresponds to the thin SITs from SMOS. The high IF in the polar hole is probably undesirable since the observations there are merely extrapolated, so in the future applications we would recommend discarding these data, in order to leave the polar hole filled instead with sea ice advected from areas where trustworthy SIT observations have been assimilated.

5. Conclusions and discussions

CS2SMOS is the first product to monitor the complete pan-Arctic SIT in a systematic way, although only for the winter months. It is a combination of two very different, yet very advanced, technologies onboard the SMOS and CryoSat-2 satellites, calibrated against very few in-situ observations of SIT, freeboard and snow depths. Altogether, the issue of measurements uncertainties is particularly delicate for the assimilation of CS2SMOS data. On the other hand, defining proper model background errors for SIT is just as delicate, when considering that the simulated SIT accumulates errors both in the sea ice dynamics (in particular the rheological model) and in the thermodynamics. The Bayesian approach to confront these two uncertainties is by Monte Carlo propagation of uncertainties, which is what is practiced in the present study for the model background error, although not for the observation error.

This study assesses the impact of assimilating the new SIT product from 19th March 2014 to 31st March 2015. Compared to the assimilated SIT CS2SMOS, the thin bias is reduced from 15 cm to 5 cm, and the RMSD also decreased from 58 cm to 38 cm, a reduction by 28.3%. Other innovation diagnostics show no degradation towards other assimilated variables –namely SIC, SSH, SST and TS profiles.

Compared to four independent drifting IMB buoys, the SITs from the two OSE runs show an overall improvement from assimilation. The benefits persist throughout the summer although no SIT observations are available then, consistently with the experiments from Mathiot et al. (2012). The assimilation reduces the low SIT biases north of the CAA and north of Greenland and the high bias in the Beaufort Sea compared to independent observations from Operation IceBridge. Both the thick pack ice in central Arctic and the thin ice in marginal seas are corrected. On average, the SIT errors in March- April of 2014 and 2015 are reduced by 14 cm, a reduction by 11.4% compared to the Official run.

The flow-dependent background errors of the EnKF method have not been demonstrated in this experiment due to the lack of ocean observations below the ice, although they may have helped avoiding degradations in the ocean. The dynamical adjustment following the assimilation of SIT has partially improved the sea ice drift speeds in the Test run where the SIT has thickened: the monthly averaged drift speed errors are reduced by 0.2-0.3 km per two days in April 2014 and January 2015. This has been revealed by satellite products but not IABP in situ buoys because of their partial coverage.

In this study, the DFS information in the ensemble data assimilation system has been applied to quantitatively evaluate the relative contributions of all assimilated observation types. CS2SMOS has the highest impact near the northern coast of Canada, north of Greenland, and on the inner side of the sea ice edge, where the contributions from CryoSat-2 and SMOS SIT were expected. The results, compared to assimilating SMOS only in Xie et al. (2016), show the importance of CryoSat-2, particularly in the winter months to constrain the SIT offsets (also proposed by Mu et al. (2018) in a coupled MITgcm model system) and motivate the assimilation of CS2SMOS in the following reanalysis of TOPAZ4.

However, some other evolutions of the modelling and observing system may reduce the impact of SIT observations. Firstly, we may hope for more in situ profiles below the sea ice, which would reduce the IF of SIC, but those are unlikely to be located in the seasonal ice zone to avoid the loss of equipment. Secondly, the SIC may have been underestimated in central Arctic due to the simplicity of the present sea ice model, further planned developments include a new model rheology that is able to resolve the scaling laws of deformation of sea ice (Rampal et al., 2016) and should therefore improve the background errors of ice concentration in winter months, increase the impact of SIC within the ice pack and comparatively effect the impact of SIT. Other planned changes such as the simulation of melt ponds are not expected to influence these results directly since there are no melt ponds when the SIT data is available.

The above OSE results, like others, are necessarily contingent on adequate specifications of observation errors. Those are very much simplified in the case of CS2SMOS, which is not an uncommon case for remote sensing observations: due to the complexity of the physics involved, the specified observation errors are reflecting interpolation errors rather than a nonlinear propagation of errors from their sources (Ricker et al., 2017). In the present study, an offset has been added to account for this difference in Eq. 6, which results in a slightly conservative error estimate with respect to the classical Desroziers optimality criterion. This means that the convergence to observed SIT could have been faster, however this would have made the EnKF less robust to the sudden changes in observations as been in Fig. 10. Further versions of the CS2SMOS data will hopefully improve their temporal continuity and the impact of the data can be increased accordingly. Since the different observation types assimilated in TOPAZ4 do not show much spatial overlap (Fig. 12 and 13), increasing the impact of CS2SMOS SIT should not decrease the performance of assimilating other data sources.

Acknowledgements

Thanks to Dr. J. Johannessen for nice suggestions and to Dr. S. Hendricks and Dr. R. Ricker for sharing the CS2SMOS data by meereisportal.de. The authors acknowledge the CMEMS support for the Arctic MFC. Grants of computing time (nn2993k and nn9481k) and storage (ns2993k) from the Norwegian Sigma2 infrastructures are gratefully acknowledged.

Reference:

Allard, R. A., Farrell, S. L., Hebert, D. A., Johnston, W. F., Li, L., Kurtz, N. T., Phelps, M.W., Posey, P.G., Tilling, R., Ridout, A. Wallcraft, A. J.: Utilizing CryoSat-2 sea ice thickness to initialize a coupled ice-ocean modeling system. *Advances in Space Research*, http://doi.org/10.1016/j.asr.2017.12.030, 2018.

Bathiany, S., Notz, D., Mauritsen, T., Raedel, G., and Brovkin, V.: On the potential for abrupt Arctic winter sea ice loss. *J. Climate*, **29**, 2703–2719, doi:https://doi.org/10.1175/JCLI-D-15-0466.1, 2016.

Bertino, L., and Lisæter, K. A.: The TOPAZ monitoring and prediction system for the Atlantic and Arctic Oceans, Journal of Operational Oceanography, 1(2), 15–19, doi: 10.1080/1755876X.2008.11020098, 2008

Bentsen, M., Evensen, G., Drange, H., and Jenkins, A. D.: Coordinate transformation on a sphere using conformal mapping, Mon. Weather Rev., 127, 2733-2740, doi:http://dx.doi.org/10.1175/1520-0493(1999)127<2733:CTOASU>2.0.CO:2, 1999.

Bouillon, S., Fichefet, T., Legat, V., and Madec, G.: The elastic-viscous-plastic method revised. Ocean Modell., 7, 2-12, doi:10.1016/j.ocemod.2013.05.013, 2013.

Budikova, D.: Role of Arctic sea ice in global atmospheric circulation: A review. Global and Planetary Change, 68,149-163, doi:10.1016/j.gloplacha.2009.04.001, 2009.

Cardinali, C., Pezzulli, S., and Andersson, E.: Influence-matrix diagnostic of a data assimilation system, Q. J. R. Meteorol. Soc., 130, 2767-2786, doi:10.1256/qj.03.205, 2004.

Chassignet, E. P., Smith, L. T., and Halliwell, G. R.: North Atlantic Simulations with the Hybrid Coordinate Ocean Model (HYCOM): Impact of the vertical coordinate choice, reference pressure, and thermobaricity, J. Phys. Oceanogr., 33, 2504-2526. Doi: http://dx.doi.org/10.1175/1520-0485(2003)033<2504:NASWTH>2.0.CO:2, 2003.

Comiso, J. C., Parkinson, C. L., Gersten, R., and Stock, L.: Accelerated decline in the Arctic sea ice cover. *Geophys. Res. Lett.*, **35**, L01703, doi:https://doi.org/10.1029/2007GL031972, 2008.

Counillon, F. and Bertino, L.: High-resolution ensemble forecasting for the Gulf of Mexico eddies and fronts, Ocean Dynam., 59, 83–95, doi:10.1007/s10236-008-0167-0, 2009.

Day, J. J., Hawkins, E., and Tietsche S.: Will Arctic sea ice thickness initialization improve seasonal forecast skill?, Geophys. Res. Lett., 41, 7566–7575, doi:10.1002/2014GL061694, 2014.

Dee, D. P., Uppala, S. M., Simmons, A. J., Berrisford, P., et al.: The ERA-Interim reanalysis: configuration and performance of the data assimilation system, Quart. J. Roy. Meteor. Soc., 137, 553-597, doi:10.1002/qj.828, 2011

Desroziers et al.: Diagnosis of observation, background and analysis-error statistics in observation space. Q. J. R. Meteorol. Soc., 131, 3385-3396, 2005.

Docquier, D., François Massonnet, F., Barthélemy, A., Tandon, N. F., Olivier Lecomte, O., and Fichefet, T.: Relationships between Arctic sea ice drift and strength modelled by NEMO-LIM3.6. The Cryosphere, 11, 2829-2846, https://doi.org/10.5194/tc-11-2829-2017, 2017

Drange, H., and Simonsen, K.: Formulation of air-sea fluxes in the ESOP2 version of MICOM, Technical Report No. 125 of Nansen Environmental and Remote Sensing Center, 1996.

Ferreira, A. S. A., Hátún, H., Counillon, F., Payne, M. R., and Visser, A. W.: Synoptic-scale analysis of mechanisms driving surface chlorophyll dynamics in the North Atlantic, Biogeosciences, 12, 3641-3653, https://doi.org/10.5194/bg-12-3641-2015, 2015.

The Cryosphere Discuss., https://doi.org/10.5194/tc-2018-101
Manuscript under review for journal The Cryosphere
Discussion started: 20 June 2018

Giles, K. A., Laxon, S. W., and Ridaut, A. L.: Circumpolar thinning of Arctic sea ice following the 2007 record ice extent mínimum. Geophys. Res. Lett., 35, L22502, doi:10.1029/2008GL035710, 2008.

Guemas, V., Wrigglesworth, E. B., Chevallier, M., et al.: A review on Arctic sea-ice predictability and prediction on seasonal to decadal time scales. Q. J. R. Meteorolog. Soc., 142(695), dio:10.1002/qj.2401, 2014.

Heygster, G., Hendricks, S., Kaleschke, L., Maass, N., et al.: L-Band Radiometry for Sea-Ice Applications, Final Report for ESA ESTEC Contract 21130/08/NL/EL. Institute of Environmental Physics, University of Bremen, 219 pages, 2009.

Hibler, W. D., III: A dynamic thermodynamic sea ice model. *J. Phys. Oceanogr.,* **9,** 817–846, 1979.

Hibler, W. D., III: Ice dynamics. chap. 9, *The Geophysics of Sea Ice,* N. Untersteiner, Ed., *NATO ASI Series B: Physics*, Plenum Press, 577–640, 1986.

Hunke, E. C., and Dukowicz, J. K.: An elastic-viscous-plastic model for sea ice dynamics, J. Phys. Oceanogr., 27, 1849-1867, doi: https://doi.org/10.1175/1520-0485(1997)027<1849:AEVPMF>2.0.CO;2, 1997.

Johannessen, O. M., Shalina, E. V., and Miles, M. W.: Satellite evidence for an Arctic Sea ice cover in transformation, Science, 286, 1937—1939. Doi:10.1126/science.286.5446.1937, 1999.

Johannessen, J. A., et al.: Toward improved estimation of the dynamic topography and ocean circulation in the high latitude and Arctic Ocean: The importance of GOCE, Surv. Geophys., 35, 661–679, doi:10.1007/s10712-013-9270-y, 2014.

Johnson, M., Proshutinsky A., Aksenov Y., Nguyen A. T., Lindsay R., Haas C., Zhang J., Diansky N., Kwok R., et al.: Evaluation of Arctic sea ice thickness simulated by Arctic Ocean Model Intercomparison Project models. J. Geophys. Res., 117(C8), doi:10.1029/2011JC007257, 2012.

Kaleschke, L., Maaß, N., Haas, C., Hendricks, S., Heygster, G., and Tonbøe, R.: A sea-ice thickness retrieval model for 1.4 GHz radiometry and application to airborne measurements over low salinity sea-ice, The Cryosphere, 4, 583-592. Doi: 10.5194/tc-4-583-2010, 2010.

Kaleschke, L., Tian-Kunze, X., Maaß, N., Ricker, R., Hendricks, S., and Drusch, M.: Improved retrieval of sea ice thickness from SMOS and Cryosat-2. Proceedings of 2015 International Geoscience and Remote Sensing Symposium IGARSS, doi: 10.1109/IGARSS.2015.7327014, 2015.

Karspeck, A. R.: An ensemble approach for the estimation of observational error illustrated for a nominal 1 global ocean model. Monthly Weather Review, 144, 1713-1728, DOI: 10.1175/MWR-D-14-00336.1, 2016.

Kern, S., Khvorostovsky, K., Skourup, H., Rinne, E., Parsakhoo, Z. S., Djepa, V., Wadhams, P., and Sandven, S., 2015: The impact of snow depth, snow density and ice density on sea ice thickness retrieval from satellite radar altimetry: results from the ESA-CCI Sea Ice ECV Project Round Robin Exercise. The Cryosphere, 9, 37-52, doi:10.5194/tc-9-37-2015.

Khvorostovsky, K., and Rampal, P.: On retrieving sea ice freeboard from ICESat laser altimeter. The Cryosphere, 10, 2329-2346, doi:10.5194/tc-10-2329-2016, 2016.

King, J., Howell, S., Derksen, C., Rutter, N., Toose, P., Beckers, J. F., Haas, C., Kurtz, N., and Richter-Menge, J.: Evaluation of Operation IceBridge quick-look snow depth estimates on sea ice, Geophys. Res. Lett., 42, 9302–9310, doi:10.1002/2015GL066389, 2015.

Kinnard, C., Zdanowicz, C. M., Fisher, D. A., Isaksson, E., Vernal, A., and Thompson, L. G.: Reconstructed changes in Arctic sea ice over the past 1,450 years. Nature, 479, 509–512. doi:10.1038/nature10581, 2011.

Kwok, R.: Simulated effects of a snow laye ron retrieval of CryoSat-2 sea ice freeboard, Geophys. Res. Lett., 41, 5014-5020, doi:10.1002/2014GL060993, 2014.

Kwok, R., and Rothrock, D.: Decline in Arctic sea ice thickness from submarine and ICESat records: 1958–2008, Geophys. Res. Lett., 36, L15501, doi:10.1029/2009GL039035, 2009.

Kurtz, N. T., Farrell, S. L., Studinger, M., Galin, N., Harbeck, J. P., Lindsay, R., Onana, V. D., Panzer, B., and Sonntag, J. G.: Sea ice thickness, freeboard, and snow depth products from Operation IceBridge airborne data, The Cryosphere, 7, 1035-1056, doi:10.5194/tc-7-1035-2013, 2013.

Laxon, S., Peacock, N., and Smith, D.: High interannual variability of sea ice thickness in the Arctic region, Nature, 425, 947-950, doi:10.1038/nature02050, 2003.

Levermann, A., Mignot, J., Nawrath, S., Rahmstorf, S.: The role of Northern sea ice cover for the weakening of the thermohaline circulation under global warming. J. Climate, 20, 4160-4171, *https://doi.org/10.1175/JCLI4232.1*, 2007.

Lindsay, R., and Schweiger, A.: Arctic sea ice thickness loss determined using subsurface, aircraft, and satellite observations, The Cryosphere, 9, 269-283, dos:10.5194/tc-9-269-2015, 2015.

Lisæter K. A., Rosanova, J. J., and Evensen, G.: Assimilation of ice concentration in a coupled ice ocean model, using the Ensemble Kalman filter. Ocean Dynamics, 53, 368-388, doi:10.1007/s10236-003-0049-4, 2003.

Lisæter, K. A., Evensen, G., and Laxon, S.: Assimilating synthetic CryoSat sea ice thickness in a coupled ice-ocean model, J. Geophys. Res., 112, C07023, doi:10.1029/2006JC003786,

The Cryosphere Discuss., https://doi.org/10.5194/tc-2018-101
Manuscript under review for journal The Cryosphere
Discussion started: 20 June 2018

2007.

Locarnini, R., Antonov, J., and Garcia, H.: World Ocean Atlas 2005, Volume 1: Temperature, vol. 61, US Dept. of Commerce, National Oceanic and Atmospheric Administration, 2006.

Martin, S., Drucker, R., Kwok, R., and Holt, B.: Estimation of the thin ice thickness and heat flux for the Chukchi Sea Alaskan coast polynya from Special Sensor Microwave/Imager data, 1990-2001, J. Geophys. Res., 109, C10012, https://doi.org/10.1029/2004JC002428, 2004.

Mathiot, P., König Beatty, C., Fichefet, T., Goosse, H., Massonnet, F., and Vancoppenolle, M.: Better constraints on the sea-ice state using global sea-ice data assimilation, Geosci. Model Dev., 5, 1501-1515, https://doi.org/10.5194/gmd-5-1501-2012, 2012.

Melia, N., Haines, K., and Hawkins, E.: Improved Arctic sea ice thickness projections using bias-corrected CMIP5 simulations, The Cryosphere, 9, 2237-2251, https://doi.org/10.5194/tc-9-2237-2015, 2015.

Mu, L., Yang, Q., Losch, M., Losa, S. N., Ricker, R., Nerger, L., and Liang, X.: Improving sea ice thickness estimates by assimilating CryoSat-2 and SMOS sea ice thickness data simultaneously. Q. J. R. Meteorol. Soc., 144(711), 529-538, DOI:10.1002/qj.3225, 2018.

Oke, P. R., and Sakov, P.: Representation error of oceanic observations for data assimilation. J. Atmos. Oceanic Technol., 25, 1004–1017, doi:10.1175/2007JTECHO558.1, 2008.

Olason, E., and Notz, D.: Drivers of variability in Arctic sea-ice drift speed, J. Geophys. Res. Oceans, 119,5755–5775, doi:10.1002/2014JC009897, 2014.

Overland, J. E., Wood, K. R., and Wang, M.: Warm Arctic—cold continents: climate impacts of the newly open Arctic Sea. Polar Research, 30, 15787, DOI:10.3402/polar.v30i0.15787, 2011.

Perovich, D. K., and Richter-Menge, J. A.: From points to Poles: extrapolating point measurements of sea-ice mass balance. *Ann. Glaciol.*, **44**, 188–192, doi:10.3189/172756406781811204, 2006.

Posey, P. G., Metzger, E. J., Wallcraft, A. J., Hebert, D. A., Allard, R. A., Smedstad, O. M., Phelps, M. W., Fetterer, F., Stewart, J. S., Meier, W. N., and Helfrich, S. R.: Improving Arctic sea ice edge forecasts by assimilating high horizontal resolution sea ice concentration data into the US Navy's ice forecast systems, The Cryosphere, 9, 1735-1745, dos:10.5194/tc-9-1735-2015, 2015.

Rampal, P., Bouillon, S., Ólason, E., and Morlighem, M.: neXtSIM: a new Lagrangian sea ice model. *The Cryosphere*, *10*(3), 1055–1073, 2016.

Ricker, R., Hendricks, S., Helm, V., Skourup, H., and Davidson, M., Sensitivity of CryoSat-2

The Cryosphere Discuss., https://doi.org/10.5194/tc-2018-101
Manuscript under review for journal The Cryosphere
Discussion started: 20 June 2018

Arctic sea-ice freeboard and thickness on radar-waveform interpretation, The Cryosphere, 8, 1607-1622, doi:10.5194/tc-8-1607-2014, 2014.

Ricker, R., Hendricks, S., Kaleschke, L., Tian-Kunze, X., King, J. and Haas, C.: A weekly Arctic sea-ice thickness data record from merged CryoSat-2 and SMOS satellite data, The Cryosphere, 11, 1607-1623, doi:10.5194/tc-11-1607-2017, 2017.

Rodgers, C.: Inverse methods for atmospheres: theory and practice, World Scientific, 2000.

Rodwell, M. J., Lang, S. T. K., Ingleby, N. B., Bormann, N., Hólm, E., Rabier, F., Richardson, D. S. and Yamaguchi, M.: Reliability in ensemble data assimilation. Quart. J. Roy. Meteor. Soc., 142, 443–454, doi: 10.1002/qj.2663, 2016.

Sakov, P., and Oke, P. R.: A deterministic formulation of the ensemble Kalman Filter: an alternative to ensemble square root filters. Tellus A, 60(2), 361-371, doi:10.1111/j.1600-0870.2007.00299.x, 2008.

Sakov, P., Counillon, F., Bertino, L., Lisæter, K. A., Oke, P. R., and Korablev, A.: TOPAZ4: an ocean-sea ice data assimilation system for the North Atlantic and Arctic. *Ocean Science*, 8(4), 633–656. http://doi.org/10.5194/os-8-633-2012, 2012.

Schofield, O., Ducklow, H. W., Martinson, D. G., Meredith, M. P., Moline, M. A., and Fraser, W. R.: How Do Polar Marine Ecosystems Respond to Rapid Climate Change? Science (328), 5985, 1520–1523, DOI: 10.1126/science.1185779, 2011.

Schweiger, A., Lindsay, R., Zhang, J., Steels, M., Stern, H., and Kwok, R.: Uncertainty in modeled Arctic sea ice volume, J. Geophys. R., 116, C00D06, doi:10.1029/2011JC007084, 2012.

Smith, G. C., Roy, F., Reszka, M., Colan, D. S., He, Z., Deacu, D., et al.: Sea ice forecast verification in the Canadian Global Ice Ocean Prediction System. Quart. J. Roy. Meteor. Soc., doi:10.1003/qj.2555, 2015.

Stark, J. D., J. Ridley, M. Martin, M., and Hines, A.: Sea ice concentration and motion assimilation in a sea ice–ocean model, J. Geophys. Res., 113, C05S91, doi:10.1029/2007JC004224, 2008.

Steele, M., Morley, R., and Ermold, W.: PHC: A global ocean hydrography with a high-quality Arctic Ocean, J. Climate, 14, 2079-2087, doi:http://dx.doi.org/10.1175/1520-0442(2001)014<2079:PAGOHW>2.0.CO:2, 2001.

Stonebridge, G., Scott, K. A., and Buehner, M.: Impacts on sea ice analyses from the assumption of uncorrelated ice thickness observation errors: Experiments using a 1D toy model, Tellus A: Dynamic Meteorology and Oceanography, 70:1, 1445379, DOI: 10.1080/16000870.2018.1445379, 2018.

Stroeve, J. C., Serreze, M. C., Holland, M. M. et al.: The Arctic's rapidly shrinking sea ice cover: a research synthesis. Climatic change, 10 (3), 1005-1027, doi:10.1007/s10584-011-0101-1, 2012.

Tian-Kunze, X., Kaleschke, L., Maaß, N., Mäkynen, M., Serra, N., Drusch, M., and Krumpen, T.: SMOS-derived sea ice thickness: algorithm baseline, product specifications and initial verification, The Cryosphere, 8, 997-1018, doi:10.5194/tc-8-997-2014, 2014.

Tilling, R. L., Ridout, A., and Shepherd, A.: Near real time Arctic sea ice thickness and volume from CryoSat-2, The Cryosphere, 10, 2003-2012, doi:10.5194/tc-10-2003-2016, 2016.

Wang, X., Key, J., Kwok, R., and Zhang, J.: Comparison of Arctic sea ice thickness from satellites, aircraft, and PIOMAS data. *Remote Sensing*, *8*(9), 1–17, http://doi.org/10.3390/rs8090713, 2016.

Woodgate, R., Aagaard, K. and Weingartner, T.: Monthly temperature, salinity, and transport variability of the Bering Strait through flow. Geophys. Res. Lett., 32, L04601, DOI: 10.1029/2004GL021880, 2005.

Xie, J., Bertino, L., Counillon, F., Lisæter, K. A., and Sakov, P.: Quality assessment of the TOPAZ4 reanalysis in the Arctic over the period 1991–2013. *Ocean Science*, 13(1), 123–144. http://doi.org/10.5194/os-13-123-2017, 2017.

Xie, J., Bertino, L., Cardellach, E., Semmling, M., and Wickert, J.: An OSSE evaluation of the GNSS-R altimetery data for the GEROS-ISS mission as a complement to the existing observational networks, *Remote Sens. Environ.*, 209, 152-165, doi:10.1016/j.rse.2018.02.053, 2018.

Xie, J., Counillon, F., Bertino, L., Tian-Kunze, X., and Kaleschke, L.: Benefits of assimilating thin sea-ice thickness from SMOS into the TOPAZ system. *The Cryosphere*, 10, 2745–2761. http://doi.org/10.5194/tc-10-2745-2016, 2016.

Xie, J., Zhu, J., Counillon, F., and Bertino, L.: Analysis of the northern South China Sea counter-wind current in winter using a data assimilation model. *Ocean Dynamics*, 65, 523-538, doi:10.1007/s10236-015-0817-y, 2015.

Table and Figures:

Table 1. Overview of observations assimilated in the official run of the TOPAZ system. All data set are retrieved from http://marine.copernicus.eu, and are assimilated weekly. The typical averaged number of observation available per assimilation cycle is reported in 4th column.

Type	Spacing	Resolution	Number of obs.	Provider
SLA	Track	7 km	10^4	CLS
SST	Gridded	5 km	10^5	OSTIA from UK Met Office
In-situ T	Point	-	10^4	Ifremer + other
In-situ S	Point	-	10^4	Ifremer + other
SIC	Gridded	10 km	10^4	OSI-SAF
Sea-ice drift	Gridded	62.5 km	10^3	OSI-SAF

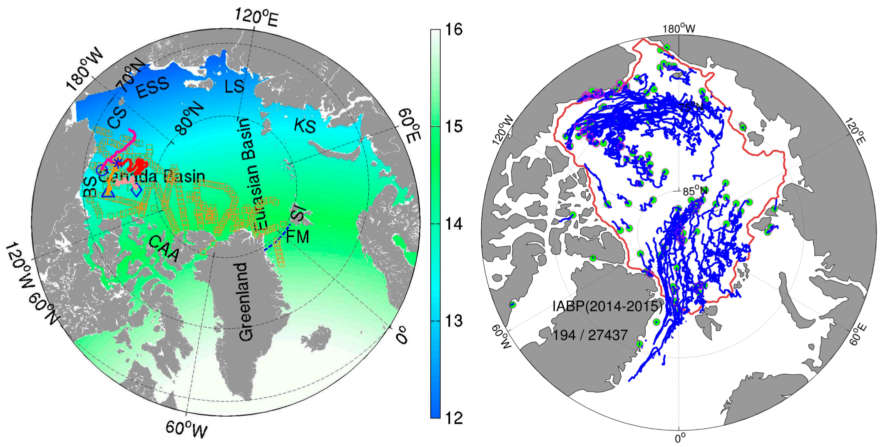

Fig. 1 Left: Horizontal resolution (km) of the model grid in the Arctic (>60°N). The black-yellow squares are the locations of IceBridge campaigns during the experimental period. The four blue markers (star, circle, triangle and diamond) are the deployment location of IMB buoys (2013F, 2014B, 2014C, and 2014F respectively). The marginal seas are: Beaufort Sea (BS), Chukchi Sea (CS), East Siberian Sea (ESS), Laptev Sea (LS), Kara Sea (KS) and the other regions: Canadian Arctic Archipelago (CAA), Svalbard Island (SI), and Fram Strait (FM; also shown with the dashed blue line). **Right**: Trajectories of International Arctic Buoy Program (IABP) buoys drift during the experimental period. The 194 buoys give their positions every 3 hours (ftp://iabp.apl.washington.edu/pub/IABP/). The green dot represents the first position in a trajectory. The solid red line excludes the coastal areas.

The Cryosphere Discuss., https://doi.org/10.5194/tc-2018-101
Manuscript under review for journal The Cryosphere
Discussion started: 20 June 2018

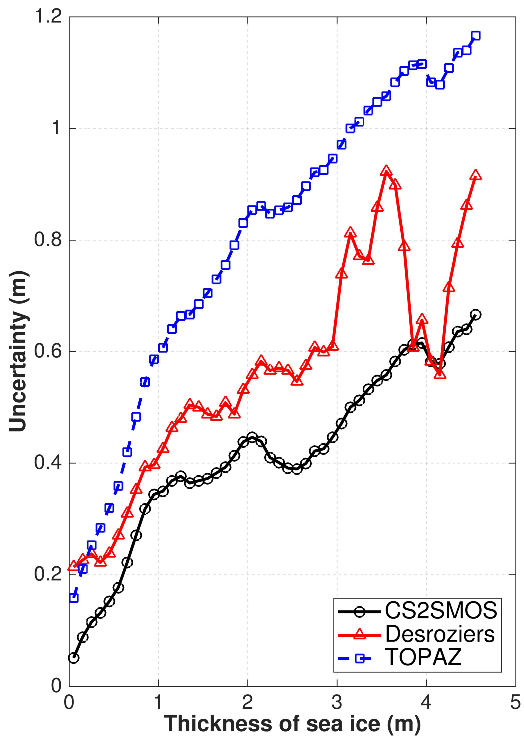

Fig. 2 Observation error uncertainties as a function of sea ice thickness for the original CS2SMOS data set (black line), the estimated observation error using the Desroziers diagnostics with red-triangle line (see Eq. 5) and the one used in TOPAZ with blue-square, with an additional term (see Eq. 6) to the original uncertainty.

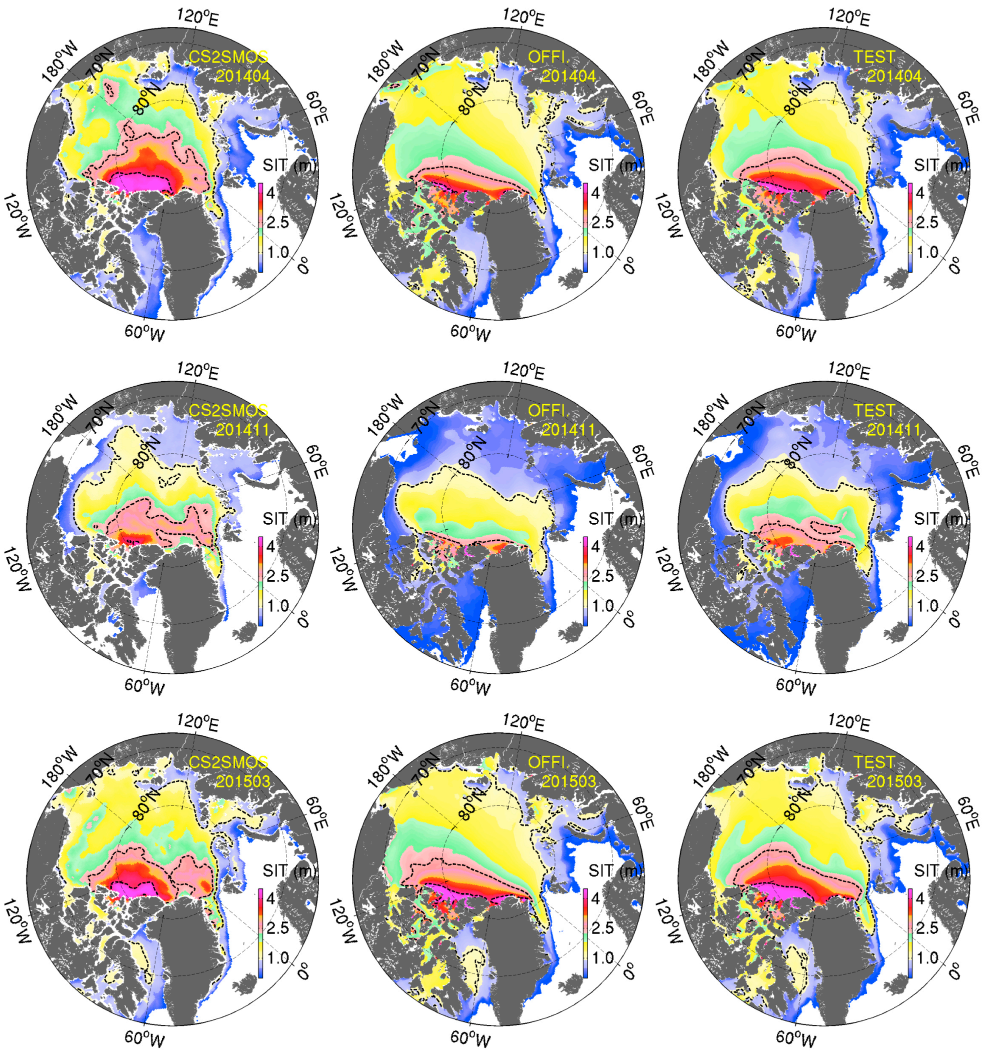

Fig. 3 Monthly SIT from CS2SMOS (left), Official run (middle) and Test run (right) in April 2014, November 2014, and March 2015. The dashed lines are isolines of 1.0, 2.5 and 4 meters SIT respectively.

The Cryosphere Discuss., https://doi.org/10.5194/tc-2018-101
Manuscript under review for journal The Cryosphere
Discussion started: 20 June 2018

The Cryosphere Discussions
Open Access

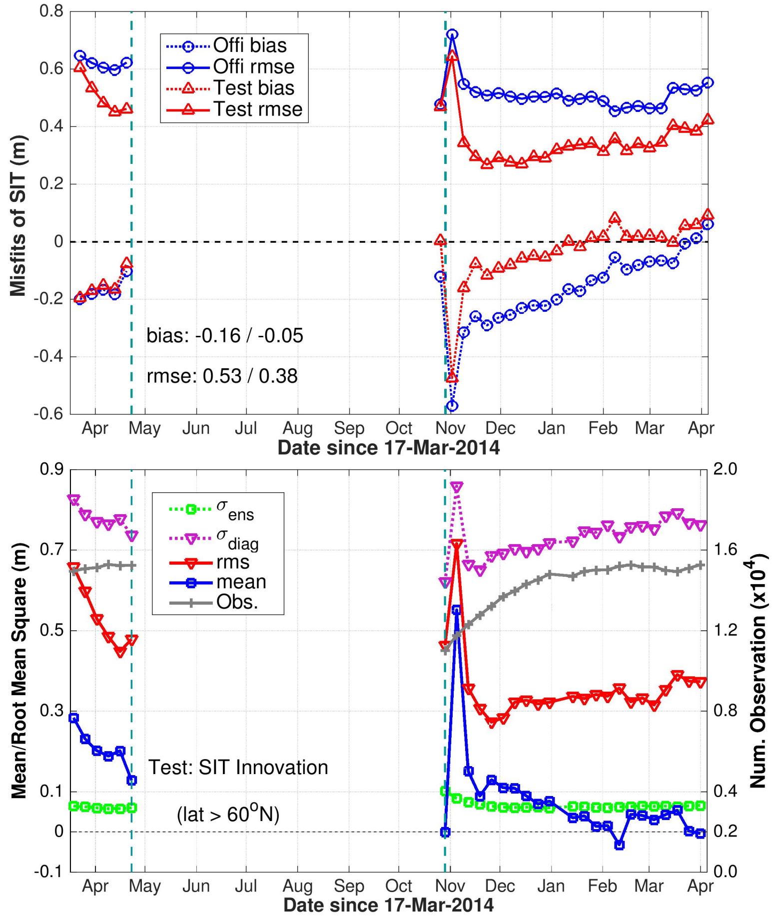

Fig. 4 Top: Bias (dotted line) and RMSD (solid line) of SIT in the two runs - Official (blue) and Test (red) – based on weekly averaged reanalysis and CS2SMOS observations. The time-averaged bias and RMSD are indicated (Official/Test). **Bottom**: SIT innovation statistics in the Test run in the Arctic region (>60°N) from 19th March 2014 to end of March 2015. The blue-squared (resp. red reverted-triangle) line represents the mean (RMS) of the innovation. The green squared line represents the ensemble spread and the purple reverted-triangle line is the diagnosed total uncertainty (see Eq. 10). The gray-crossed line is the number of assimilated observations.

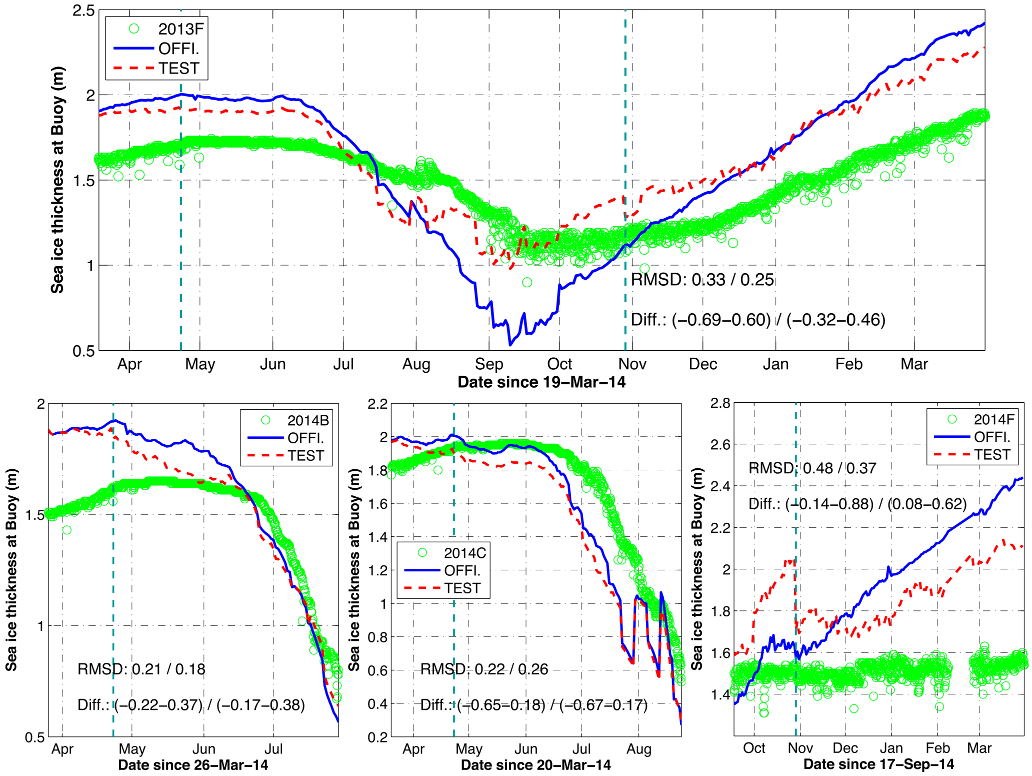

Fig. 5 Time series of SIT along the trajectories of IMB buoys (upper: 2013F; bottom: 2014B, 2014C, and 2014F). Measured SIT (green), daily averages from the Official run (blue line) and the Test run (red line). The vertical cyan-dashed lines indicate the winter period when C2SMOS is assimilated in the Test run.

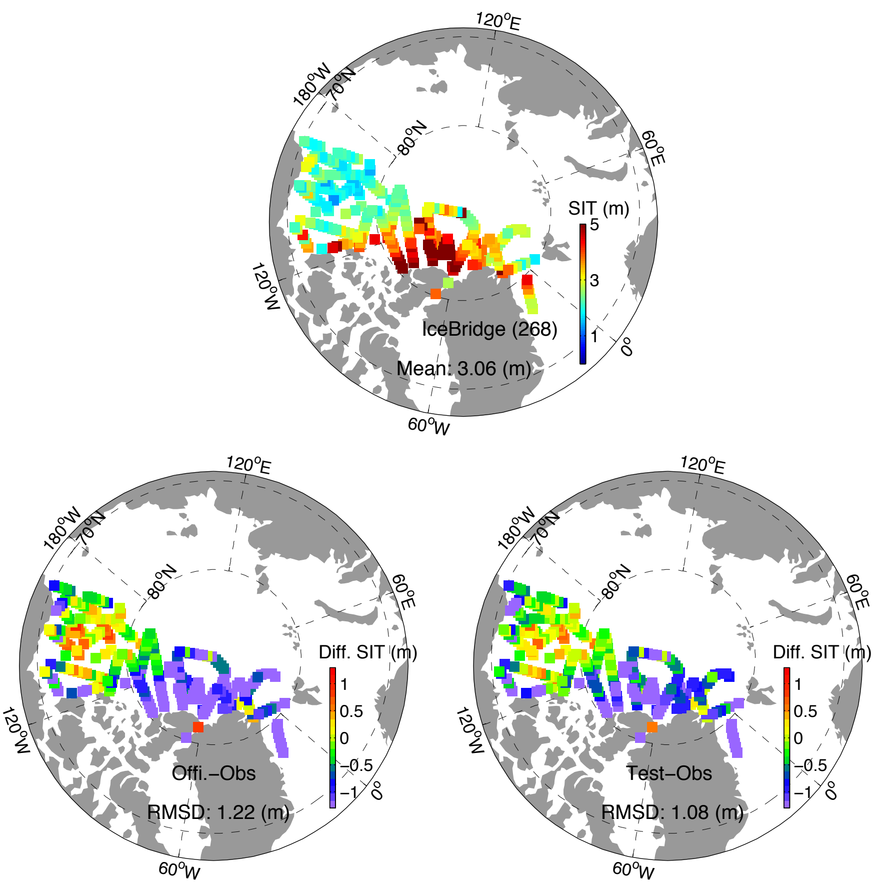

Fig. 6 Top: IceBridge SIT in both 2014 and 2015. **Bottom**: deviations from the Official run (left) and Test run (right) using model daily average at observations time.

The Cryosphere Discuss., https://doi.org/10.5194/tc-2018-101
Manuscript under review for journal The Cryosphere
Discussion started: 20 June 2018

The Cryosphere
Discussions
Open Access

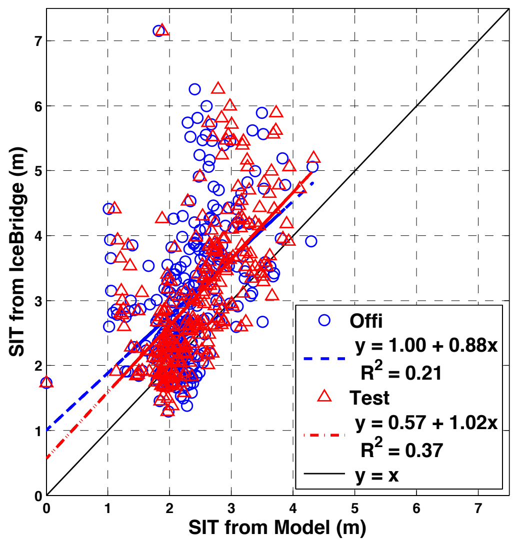

Fig. 7 Scatterplots of SIT daily averaged of Official (blue) and Test (red) runs compared to IceBridge data. The dashed lines are after linear regression respectively. The black line is y=x.

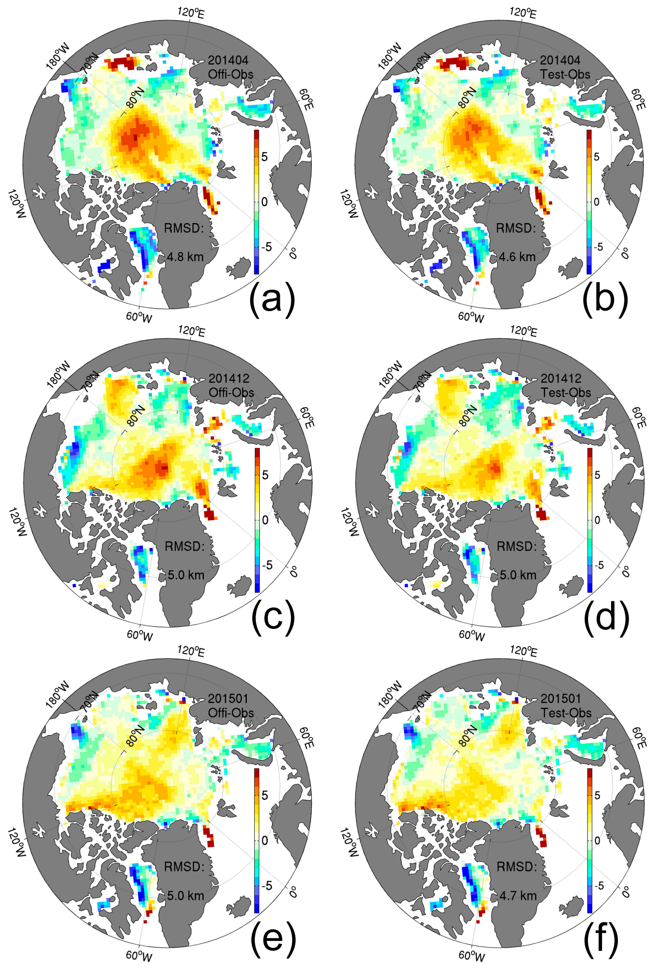

Fig. 8 Sea ice drift misfits (model minus observation, in km per two days) in the Official run (left column) and Test run (right column) compared against the OSI-SAF sea ice drift in April 2014 (panels a and b), December 2014 (panels c and d), and January 2015 (panels e and f).

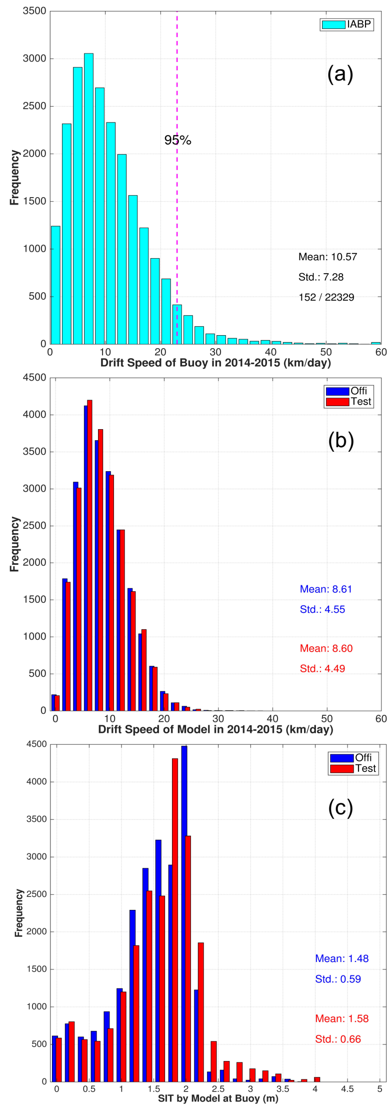

Fig. 9 (a) Histogram of sea ice drift speeds calculated from IABP buoys for the period 2014-2015; Over 95% sea ice drift speeds are slower than 24 km/day. (b) histogram of the drift speed in the Official (blue) and Test (red) runs; the mean speed and the standard deviation are indicated; (c) histogram of the simulated SIT at the buoy locations from the two runs.

The Cryosphere Discuss., https://doi.org/10.5194/tc-2018-101
Manuscript under review for journal The Cryosphere
Discussion started: 20 June 2018

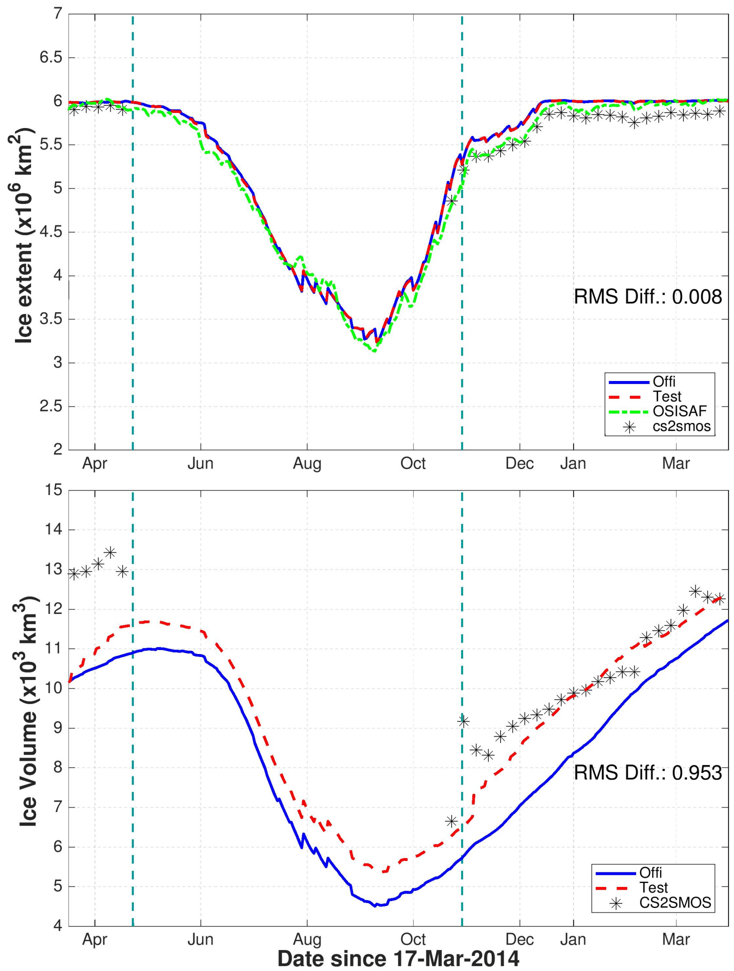

Fig. 10 SIE and SIV in the official run (blue), the test run (blue) and satellite observations in the Central Arctic. The black stars are weekly SIE (or SIV) from CS2SMOS. The green dash-dotted line is the daily SIE from OSI-SAF. The averaged differences of the two runs (Offi.-Test) are reported. The vertical cyan-dashes mark the periods when C2SMOS data is assimilated.

The Cryosphere Discuss., https://doi.org/10.5194/tc-2018-101
Manuscript under review for journal The Cryosphere
Discussion started: 20 June 2018

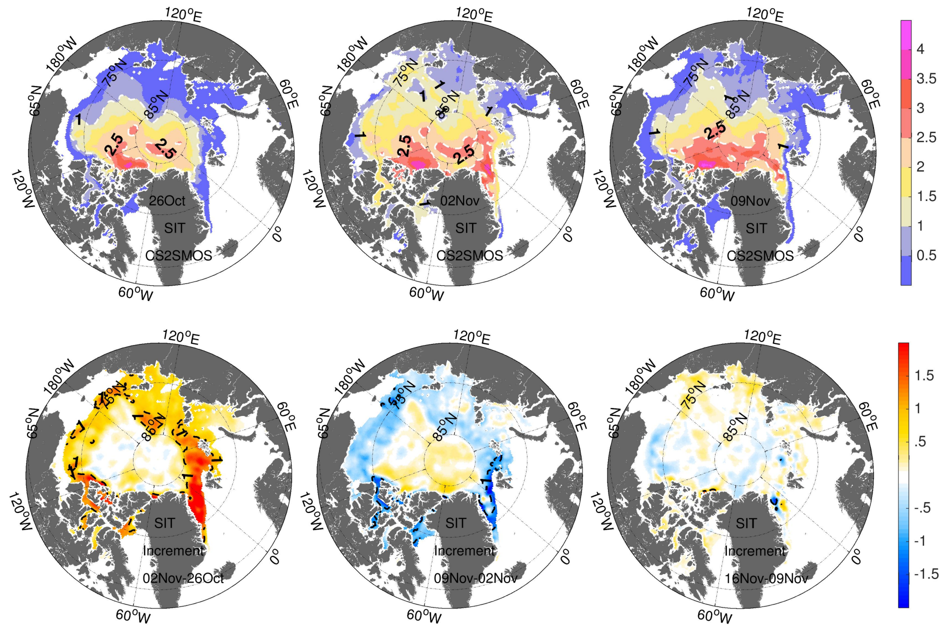

Fig. 11 **Top**: First three weekly SIT from CS2SMOS in the beginning of fall 2014. The dashed white lines denote the 1 and 2.5 m isolines. **Bottom**: The associated time increments of SIT. The dashed lines denote the -1 and 1 m isolines.

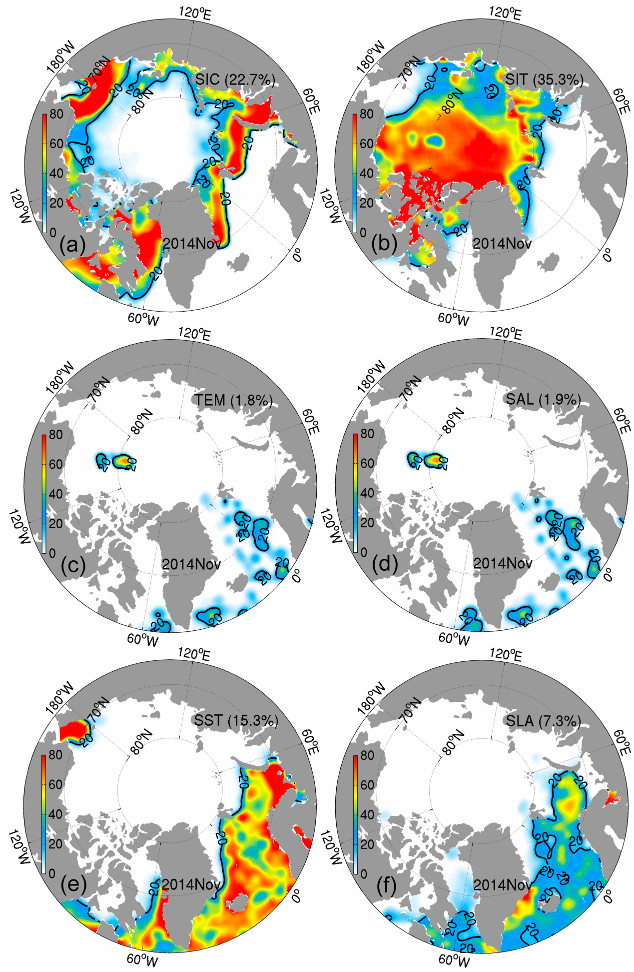

Fig. 12 Relative DFS contributions of each observation data types in November 2014. (a) SIC from OSI-SAF; (b) SIT from CS2SMOS; (c) temperature profiles; (d) salinity profiles; (e) SST; (f) along-track sea level anomaly (SLA). The black line is the 20% isoline, and the monthly IF (see Eq. 15) is reported between parenthesis.

The Cryosphere Discuss., https://doi.org/10.5194/tc-2018-101
Manuscript under review for journal The Cryosphere
Discussion started: 20 June 2018

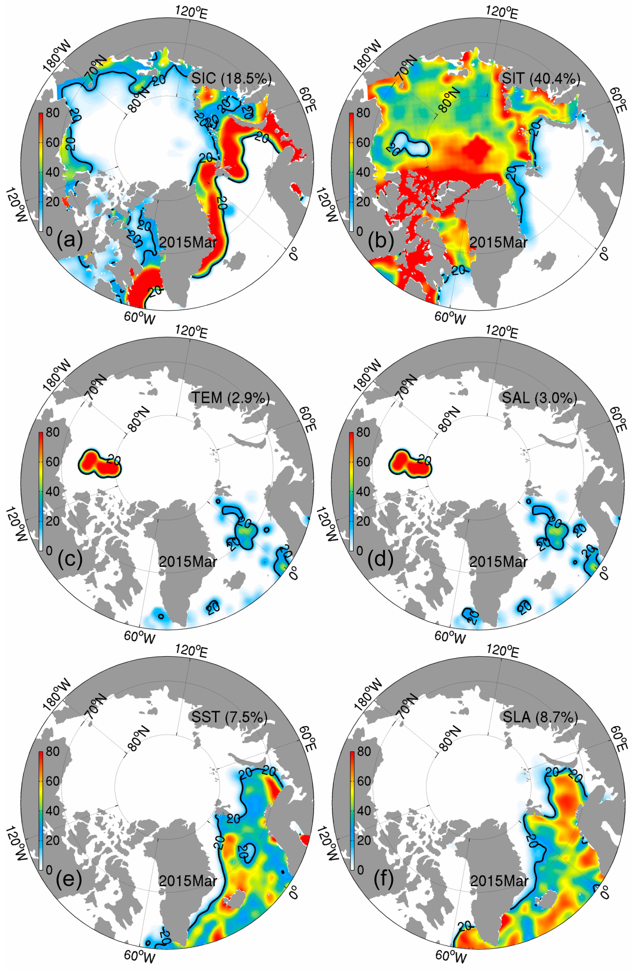

Fig. 13 Same as the above but in March 2015.